Nanotechnology Perceptions
ISSN 1660-6795
www.nano-*ntp.com*

Multifunctional Silver, Zirconia And Graphene-Doped Tio$_2$ Nanotube Arrays Via In-Situ Anodization For Enhanced Antibacterial And Antibiofilm Implant Interfaces

R.Hemalin Subala[a,f], D. Henry Raja[b,f], D. Jonas Davidson[c], M.Amalanathan[d*,f], M. Sony Michael Mary[e,f]

[a]*Research Scholar, Reg.No.21123162132016, Department of Physics, Scott Christian College, Nagercoil 629001, Tamil Nadu, India.*
[b]*Department of Physics, Scott Christian College, Nagercoil 629003, Tamil Nadu, India*
[c]*Senior Principal Scientist, CSIR-CECRI, Karaikudi, Tamil Nadu, India.*
[d*]*Department of Physics & Research Centre, Nanjil Catholic College of Arts & Science, Kaliyakkavilai-629 153, Tamil Nadu, India.*
[e]*Department of Physics, Annai Velankanni College, Tholayavattam -629157, Tamil Nadu, India.*
[f]*Affiliated to Manonmaniam Sundaranar University, Abishekapatti, Tirunelveli-627 012 Tamil Nadu, India.*

A major threat to world health is antimicrobial resistance,which has an effect on the performance of medical apparatus that are defenceless risk of implant-associated infections and biofilm establishment.Using an in -situ anodization technique,titanium dioxide (TiO_2) nanotube arrays doped with graphene (G),zirconia(Zr), silver (Ag),and their mixtures are synthesized and thoroughly evaluated in this work. Phase retention,morphological homogeneity,and successful doping were validated by FESEM,EDX,and XRD characterization. Ag-doped TiO_2 nanotubes showed the strongest antibacterial activity against Pseudomonas aeruginosa,according to antibacterial tests. This feature was explained by mechanisms including membrane rupture and silver ion release. Co-doped zirconia-graphene nanotubes demonstrated strong antibiofilm effectiveness by combining bacterial suppression with mechanical stability. These multifunctional doped TiO_2 nanotube coatings have the potential to reduce implant-associated infections by exhibiting long-lasting antibacterial and antibiofilm properties at the local level. This study highlights how tailored nanostructured surfaces can be used to advance implant technologies that are resistant to drugs.

1. INTRODUCTION

Antibacterial activity has emerged as a critical area of research because of the concerning increase in antimicrobial resistance (AMR) and the related risk of infections during medical procedures and with implantable devices. Projections by the WHO suggest that, if left unaddressed, antimicrobial resistance may surpass cancer inmortality rates by mid-century,

potentially causing up to 10 million deaths annually[1]. Pathogens evade conventional antibiotics through resistance mechanisms like active efflux systems, enzymatic degradation (e.g., β-lactamases) and biofilm formation [2].These threats jeopardize the success of surgeries, chemotherapy, and organ transplants, all of which rely on effective antibacterial protections [3].

As noted in WHO reports,"MRSA, multidrug-resistant Psedomonas aeruginosa, and carbapenem-resistant Enterobacteriaceae are just a few of the multidrug resistant strains that have emerged due to extensive misuse of antibiotics" [4]. At the same time, pharmaceutical companies have scaled back antibiotic development because of economic and regulatory constraints, creating a "discovery void" [5]. International travel and trade continue to accelerate the global spread of resistant bacteria [6].

Medical implants and devices are particularly susceptible to bacterial colonization. Conventional sterilization methods provide limited, short-term protection and are ineffective against biofilm-associated infections. Biofilms, which are structured microbial assemblies embedded in a matrix of extracellular polymers, exhibit extreme resistance to antibiotics-often requiring concentrations hundreds to thousands of times greater than those effective against free-floating bacteria. This resilience contributes significantly to persistent infections associated with medical implants, underscoring the need for surface materials that possess both antibacterial and antibiofilm capabilities[7,8]. Among current approaches, titanium dioxide (TiO_2) nanotubes prepared by anodization have emerged as promising implant surface modifications. TiO_2 is valued for its corrosion resistance, osteoconductivity, and biocompatibility, while nanotubular structures provide large surface area, tunable morpholpgy, and excellent platforms for loading antibacterial agents [9]. In addition, TiO_2 nanotubes support localized, sustained antibacterial activity directly at the implant interface, reducing reliance on systemic antibiotic use [10].

The anodization technique represents a versatile, cost-effective, and scalable route for developing structured TiO_2 nanotube configurations. By precisely tuning electrochemical oxidation variables like applied potential, processing time, and electrolyte formulation, the nanotube diameter, length, and wall thickness can be controlled, which directly influences their biological activity and antibacterial performance [11]. Electrolyte formulation plays a critical role in nanotube development. Although fluoride-based electrolytes are commonly employed to initiate self-organized nanotube formation, the incorporation of ammonium chloride (NH_4Cl) enhances ionic conductivity, stabilizes oxide growth, and promotes uniform tube morphology by balancing field-assisted oxidation and chemical dissolution processes [12]. Such well-structured nanotubes offer an increased surface area and highly reactive sites for incorporation of antibacterial dopants -including silver, zirconia, and graphene-thereby augmenting both antibacterial and antibiofilm functions at the implant interface.

Silver enhances the antibacterial efficacy of TiO_2 by damaging bacterial membranes, inducing oxidative stress via ROS generation, and interfering with DNA replication mechanisms [13].When incorporated into TiO_2 nanotubes, Ag ions can be gradually released, preventing bacterial adhesion and biofilm initiation while maintaining low cytotoxicity [14]. Recent studies show that Ag-doped TiO_2 nanofilms achieved 99.7% antibacterial efficiency on vascular implants via combined Ag ion release and photocatalytic ROS generation [15].

Silver-loaded TiO_2 nanotube arrays prepared by anodization and ion implantation also demonstrated long-term antibacterial and osteogenic effects [16].

Beyond silver, the incorporation of zirconia and graphene further strengthens antibacterial and antibiofilm properties. Zirconia enhances mechanical stability, chemical durability, and biocompatibility, while graphene exerts antimicrobial effects by physically disrupting bacterial membranes, including oxidative stress, and hindering biofilm development [17,18]. Their synergistic integration with TiO_2 nanotubes results in multifunctional coatings with superior antibiofilm activity, structural stability, and favourable biological interactions.

Therefore, the development of Ag-doped and zirconia/graphene-modified TiO_2 nanotubes, fabricated through scalable in-situ anodization, represents a promising strategy to combatz implant-associated infections. These multifunctional nanostructured coatings are anticipated to combine antibacterial and antibiofilm efficacy with excellent biocompatibility, thus advancing the design of next-generation biomedical implants. In this study, we systematically evaluate undoped and doped TiO_2 nanotubes to elucidate the individual and synergistic roles of silver, zirconia, and graphene in modulating antibacterial and antibiofilm capability**.**

2. Experimental section

2.1 Materials

High- purity titanium foil (99.7%, dimensions: 3 cm x 1 cm x 0.25 mm)sourced from Sigma-Aldrich (USA) served as the working electrode for anodization. Ethylene glycol $C_2H_6O_2$, 99%) and ammonium fluoride (NH_4F, 98%) were procured from SRL Chemical (India). Zirconium oxychloride ($ZrCl_2.xH_2O$) and graphene nanoparticles were obtained from respective manufacturers. Silver nitrate ($AgNO_3$), acetone (C_3H_6),AR grade), and absolute ethanol (C_2H_6O,AR grade) were acquired from commercial sources. All reagents used were of analytical grade and employed without further purification. Deionized water for all procedures was sourced from a Millipore Milli-Q system.

2.2 Synthesis of Undoped and Doped TiO_2 Nanotube Arrays via the Anodization

Undoped titanium dioxide (TiO_2) nanotube arrays were prepared via the anodization using the above titanium foil as the substrate. Prior to anodization, the titanium substrates underwent ultrasonic treatment in acetone, ethanol, and deionized water, each for duration of 10 minutes, and were then dried at room temperature. The rear surface of the titanium foil was insulated using Scotch tape and Parafilm to ensure unidirectional anodization.

The electrolyte was formulated by dissolving 0.5 wt% NH_4F and adding 2 vol% deionized water into 40 ml of ethylene glycol. Anodization was performed at ambient temperature under a constant voltage of 30V for 90 minutes using an Alpab DC power source. Post-anodization, the samples were rinsed thoroughly with ethanol and distilled water, and then air-dried.Thermally annealing was conducted at 490^0C for 3 hours to enhance crystallinity and structural integrity.

For the doped samples, precursor materials were added into the electrolyte prior to the anodization process. For Ag doping, a calculated amount of silver nitrate ($AgNO_3$) was

introduced into the electrolyte. Graphene-doped TiO_2 nanotubes were synthesized by dispersing graphene nanoparticles in the anodizing solution. Zirconia doping was achieved by adding zirconium oxychloride ($ZrOCl_2.xH_2O$), while co-doping with zirconia and graphene was carried out by adding both zirconium oxychloride and graphene nanoparticles simultaneously. All doped samples followed the same anodization parameters and annealing protocol as the undoped control.
The sample code used throughout this study are summarized in below

Table 1. Sample code and their descriptions

Sample Name	Description
B	Bare (Undoped) TiO_2 nanotubes
S	Silver (Ag) doped -TiO_2 nanotubes
ZG	Zirconia-graphene co-doped TiO_2nanotubes
G	Graphene doped TiO_2 nanotubes
Z	Zirconia doped - TiO_2 nanotubes

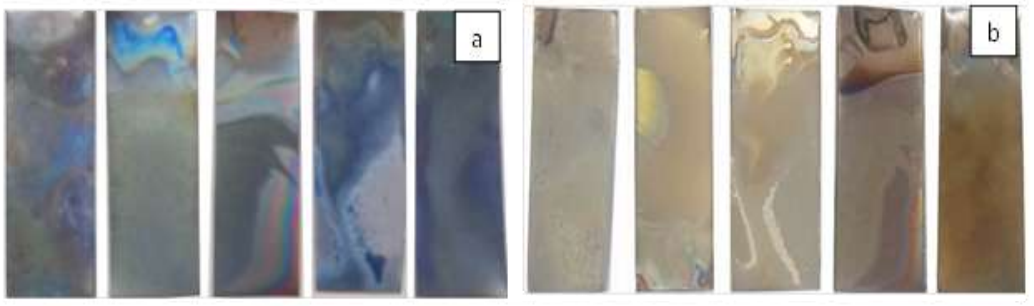

Figure 1. Surface morphology of TiO_2 nanotube samples a)before annealing and b) after annealin

2.3 Characterization

The structural and compositional features of the synthesized TiO2 nanotube arrays were thoroughly examined at CSIR-Central Electrochemical Research Institute (CSIR), Karaikudi. Field Emission Scanning Electron Microscopy (FESEM) and Energy Dispersive X-ray Spectroscopy (EDX) were employed to investigate surface morphology and elemental distribution, respectively. Morphological analysis was conducted using a Carl Zeiss SUPRA 55VP FESEM,equipped with a Gemini column, operated at an accelerating voltage of 5 kV and a working distance of approximately 9 mm, enabling high-resolution imaging down to 1.2 nm. Elemental profiling was carried out using an Oxford Instruments X-MAX system, which detects characteristic X-rays emitted upon electron beam interaction, providing both qualitative and semi-quantitative elemental data. Crystallographic properties were assessed using a Bruker D8 ADVANCE X-ray diffractometer with CuKα radiation (λ=1.3417

A^0),functioning at 40 kV and 30 mA. Diffraction data were recorded across a 2θ range of 20° to 30°with a step size of at 0.020. The resulting patterns were interpreted using standard JCPDS reference files to determine phase identity, crystallite dimensions, lattice constants,and miller indices.

2.4 Antibacterial Activity

The antibacterial properties of the prepared samples wereassessed using the agar well diffusion technique against Pseudomonas aeruginosa (MTCC 424), sourced from MTCC, Chandigarh, India. Nutrient agar from HiMedia (India) was made by dissolving 2.8 grams in 100 mL of distilled water, followed by sterilization at 121° C for 15 minutes through autoclaving.Subsequently, 25-30 mL of the medium was dispensed into sterile Petri plates.Nutrient broth was similarly prepared and used to grow the bacterial culture. A 24-hour culture P.aeruginosa was standardized to 0.5 McFarland turbidity before being evenly applied onto the surface of solidified agar plates. Circular wells (6 mm in diameter) were aseptically created in the medium, and varying concentrations of the samples (B, S, ZG, G, and Z) were dispensed into them. Following sample application, the inoculated agar plates were maintained at 37^0C for 24 hours to allow bacterial growth and interaction with the test materials. Post-incubation, the inhibition zones surrounding each well were measured in millimeters to assess antibacterial efficacy. All experiments were conducted in triplicate to ensure reproducibility, and the resulting data were statistically analyzed using GraphPad Prism version 6.0 (GraphPad softare Inc.,USA).

2.5 Antibiofilm Activity

This study investigated the antibiofilm efficacy of titanium dioxide nanotubes doped with silver (TiO_2-Ag) and zirconia-graphene (ZG) nanomaterials against pathogenic bacteria using the standard microtiter plate (MTP) assay [19]. Overnight bacterial cultures grown in BHI broth at 37^0C were inoculated into 96-well flat-bottom polystyrene plates containing 180 µL of fresh BHI broth and 10 µL of culture, followed by the addition of 10 µL of either TiO_2-Ag,ZG, or sterile water (control). After 24 hourincubation at 37°C, planktonic bacteria were carefully removed from the plate by washing with phosphate-buffered saline (PBS).The remaining sessile cells were then fixed using a 2% sodium acetate solution, followed by staining with 0.1% crystal violet. Subsequently,excess stain was washed away with deionized water and the plates were left to air dry.The amount of crystal violet retained by the biofilm was quantified spectrophotometrically at 600 nm using a Thermo Scientific microplate reader. Biofilm inhibition was determined as a percentage using a standard calculation formula.

$$\text{Percentage inhibitionof biofilm formation} = \frac{OD_{(Control)} - OD_{(sample)}}{OD_{(Control)}} \times 100$$

All experiments were conducted in three independent replicates, and the data were presented as mean values with corresponding standard deviation. The study adhered to Biosafety Level 2 (BSL-2) protocols, utilizing appropriate personal protective equipment (PPE), and all chemical and nanomaterial waste was disposed of following approved safety and environmental guidelines.

3.1 XRD analysis

Over a 2θ range of 10°–80°, the bare and doped TiO_2 samples' X-ray diffraction (XRD) patterns were captured using Cu Kα radiation (λ = 1.5406 Å). The anatase phase was characterized by high diffraction peaks in the undoped TiO_2 (sample B). The most prominent peak was located at about ~25.3°, which corresponds to the (101) plane (JCPDS No. 21-1272). Further peaks were found at 37.8°, 48.0°, 53.9°, and 55.1°, equivalent to the (004), (200), (105), and (211) planes, respectively. The lack of rutile, brookite, or metallic titanium phases confirmed phase purity (JCPDS No.44-1294) [20]. The average crystallite size of TiO2 was calculated using the Debye-Scherrer formula, based on the extent of peak broadening observed in the X-ray diffraction patterns.(Figure 2).

$$D = k\lambda \div \beta\cos\theta$$

In this case, β stands for full width at half maximum (FWHM), θ for angle of diffraction, λ for wavelength (1.5417 Å), D for crystalline size, and k for the Scherrer constant (0.9) (Debye-Scherrer formula). The crystallite size in the undoped sample was approximately 32.4 nm. Minor shifts and unexpected peaks that were consistent with dopant incorporation were still present in the doped samples' anatase structure.

Sample S, which was silver-doped TiO_2, showed an extra peak at about 38.4°, indicating the presence of JCPDS No. 04-0783[21]. The diameter ranged from 28.6 to 198 nm. Zirconia and graphene co-doped TiO_2 (sample ZG) had a broad peak near 26.6° that was characteristic of graphene and a peak at 35.2° that was indexed to the (110) plane of tetragonal ZrO_2 (JCPDS No. 80-0965)[22-23]. The range of the crystallite size was 17.9 and 145 nm. Sample Z, zirconia-doped TiO_2 showed anatase peaks without distinct ZrO_2 reflections, indicating lattice substitution: the crystallite size was around 14.3 nm[24]. Successful dopant incorporation, anatase phase retention, and crystallinity changes that directly affect functional characteristics are all confirmed by this thorough investigation.

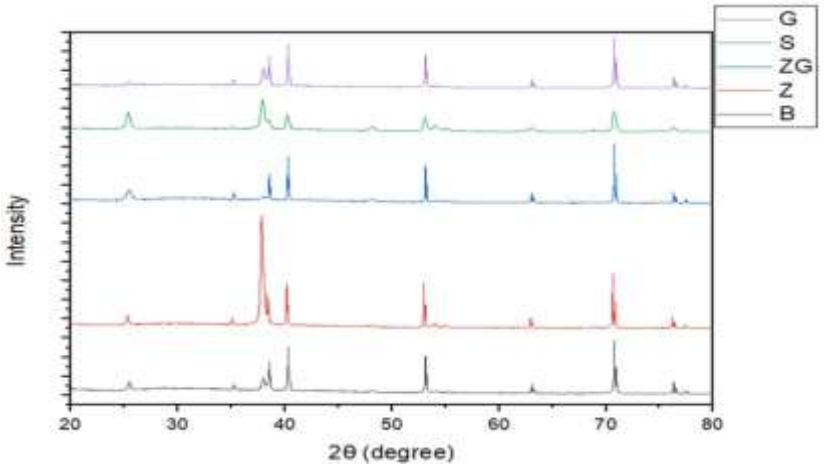

Figure 2. X-ray diffraction spectrum indicating crystalline phases of doped TiO_2

Table 2. Key XRD peak positions (2θ), calculated crystallite sizes, and notable features for bare and doped TiO_2 samples.

Sample	Key XRD peaks (20.º)	Crystallite size	Notable features
B	25.3 (101),37.8,48.0,53.9,55.1	~ 32.2	Pure antase phase, Nanocrystalline
S	25.3,37.8,38.4(Ag º),48.0,53.0,55.0	17.9-145	Metallic Ag peak, enhanced crystallinity
ZG	25.4,37.9,38.5,40.3,53.1,26.6(graphene)	28.6-198	ZrO2 peak at 35.2 º graphene presence
G	25.3,37.9,48.1,53.0,55.1,26.0-26.6(graphene)	~21.6	Graphene prak,anatase Phase

3.2 FESEM analysis

The TiO2 nanotube arrays formed via in-situ anodization in an ammonium fluoride-containing electrolyte were subsequently subjected to annealing at 490°C for one and a half hours to achieve the desired crystallinity.

The TiO_2 nanotube arrays formed via in-situ anodization in an ammonium fluoride-containing electrolyte were subsequently subjected to annealing at 490ºC for one and a half hours to achieve crystalinity. The development of uniformly aligned, vertically oriented nanotube morphologies in all samples was validated by FESEM characterization (figure 3.1). The test specimen was the undoped sample (B), which showed homogeneous nanotubes with an average wall thickness of 12 nm, an outer diameter of 86 nm, and an interior diameter of roughly 61 nm [25,26]. These values were determined using Image J software for precise measurement of FESEM images.

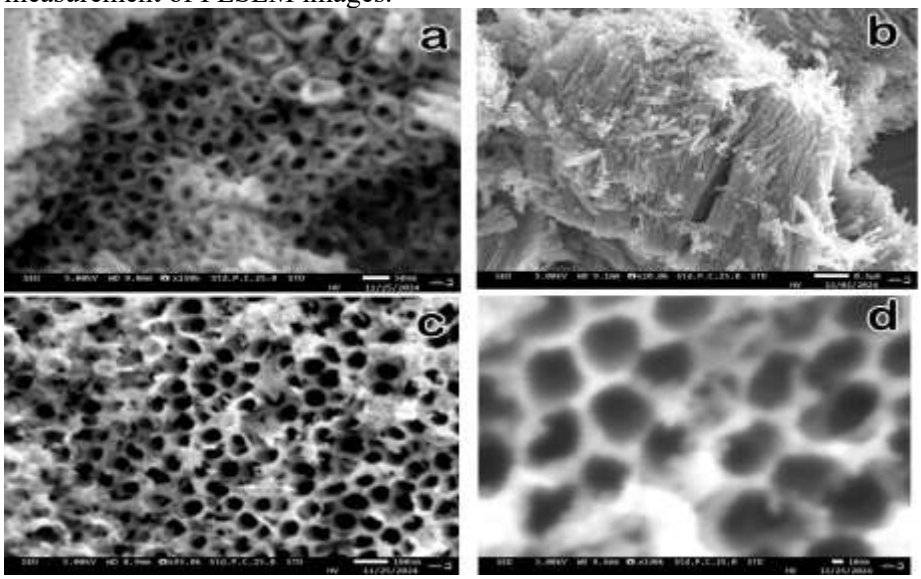

Figure 3.1 Field Emission Scanning Electron Microscope (FESEM) images of TiO2 nanotbe samples (a) top view of bare (undoped) sample; (b) vertical view of bare sample; (c) top view of silver-doped sample; (d) vertical view of silver-doped sample

The maximum tube length (~2µm) and the thinnest walls (~7 nm) were found in silver-doped nanotubes (sample S), highlighting the potential of silver to enhance antibacterial activity and enhance oxide dissolving. The most compact nanotube architecture was shown by the co-doped sample ZG (zirconia and graphene), which had an average wall thickness of about 12 nm and inner and outer diameters of 24 and 39 nm, respectively. According to this study, zirconia and graphene in collaborate to optimize morphology without sacrificing the nanotubes' structural alignment. Nanotube dimensions were somewhat reduced by graphene doping (sample G), with inner and outer diameters of roughly 55 nm and 83 nm, respectively, and a lowered wall thickness of roughly 9 nm. This study is in line with other research and implies that graphene has a moderating effect on nanotube development.

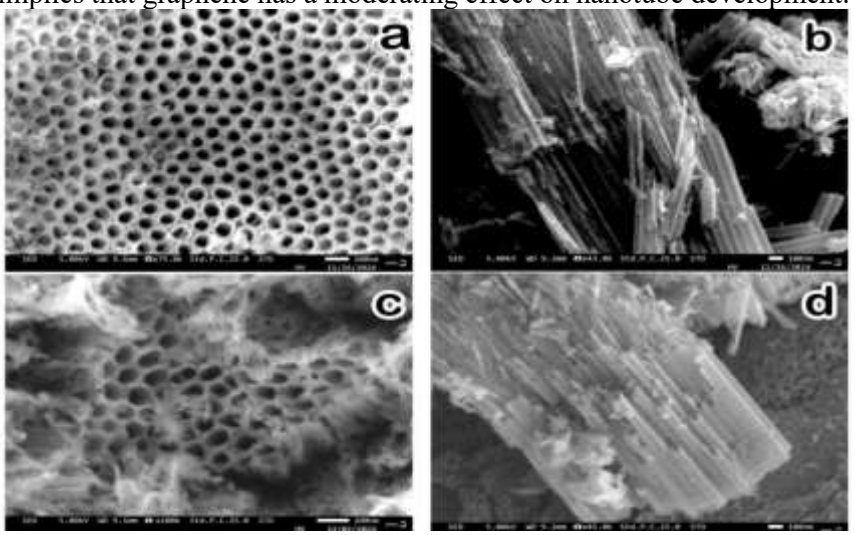

Figure 3.2. Field Emission Scanning Electron Microscope (FESEM) images of doped TiO2 nanotube samples.(a) Top view of ZG (zirconia and grapheme co-doped) sample; (b) vertical view of Z (zirconia-doped) sample; (c) top view of G (grapheme –doped) sample; (d) vertical view of Z (zirconia=doped) sample.

Further dimensional reduction was achieved by zirconia doping (sample Z), producing thinner tubes with inner and outer diameters of roughly 51 and 65 nm, respectively, and a wall thickness of about 6 nm [27-31]. These morphological changes, mainly the smaller nanotube sizes and higher aspect ratios seen in doped materials, should greatly boost surface reactivity when taken together. Figure 3.2 displays representative FESEM images of ZG,Z,and G doped with TiO2 nanotube samples in both vertical and top views.

In accordance with known antibacterial mechanisms involving doped TiO_2 nanotubes, such structural features may improve antibacterial efficacy through enhanced contact-mediated interactions and ionic release.

Table 3. Lists the main morphological characteristics of the bare and doped TiO_2 samples along with structural parameters (inner/outer diameter, wall thickness)

Sample	Inner diameter (nm)	Outer diameter (nm)	Wall thickness (nm)	Key features
B	≈ 61	≈ 86	≈ 12	Well aligned structure
S	≈ 60	≈ 80	≈ 7	Thinnest walls, Largest tubes (≈2µm),
ZG	≈ 24	≈ 39	≈ 12	Most compact
G	≈ 55	≈ 83	≈ 9	Smooth walls,reduced size due to grapheme
Z	≈ 51	≈ 65	≈ 6	Strong tube definition, mechanically robust

3.3 EDX analysis

The successful in-situ doping of the TiO_2 nanotube arrays with the desired elements is confirmed by the EDX analysis of all samples. The exceptional purity of the undoped reference material was confirmed by sample B, which solely displayed Ti and O. Sample S confirmed silver doping by showing the distinctive Ag peak with little contamination [32]. C. Zr, Ti, and O were all detected simultaneously in sample ZG, demonstrating dual doping with graphene and zirconia. Graphene inclusion was confirmed by sample G, which showed a clear C signal next to Ti and O. Successful zirconia doping was indicated by sample Z, which showed distinct Zr peaks in addition to Ti and O. All samples show no discernible undesired element peaks, demonstrating the compositional control attained by the anodization process and confirming the efficacy of the synthesis approach. Representative EDX spectra for the doped TiO2 nanotube samples are shown in Figure 4.1. The selected analysis areas for these samples are displayed in figure 4.2. For comparison, the EDX spectrum and analysis area for the undoped samples are presented in figure 4.3..It is anticipated that these compositional differences will affect each sample's antibacterial activity, with dopants like Ag, graphene, and Zr enhancing antimicrobial processes through better conductivity, structural stability, and ionic interactions [33-35].

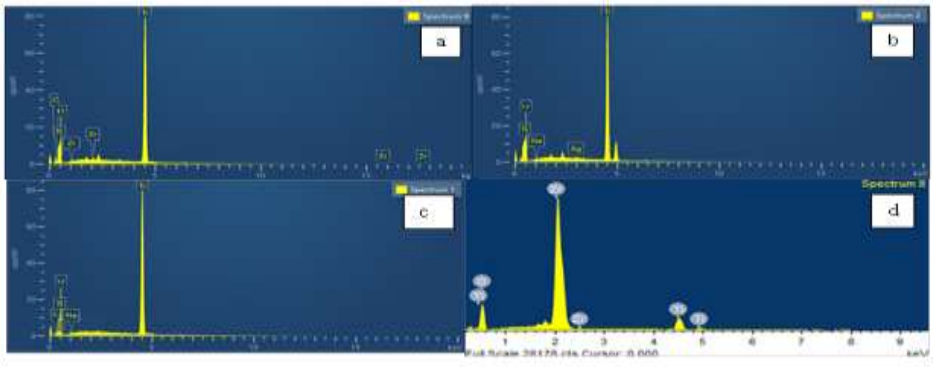

Figure 4.1. EDX spectra of doped TiO_2 nanotube samples; (a) ZG (zirconia and grapheme co-doped), (b) S (silver –doped), (c) G (grapheme-doped),and (d) Z (zirconia –doped) samples.

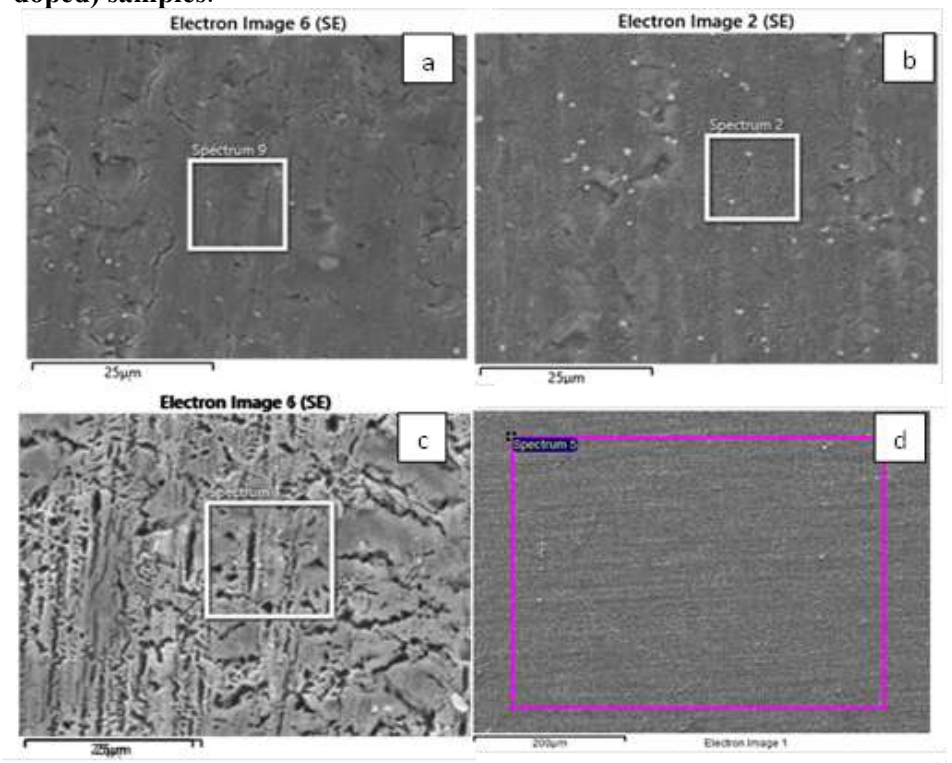

Figure 4.2. Selected analysis areas for EDX on doped TiO_2 nanotube samples (a) ZG, (b) S, (c)G, (d) Z

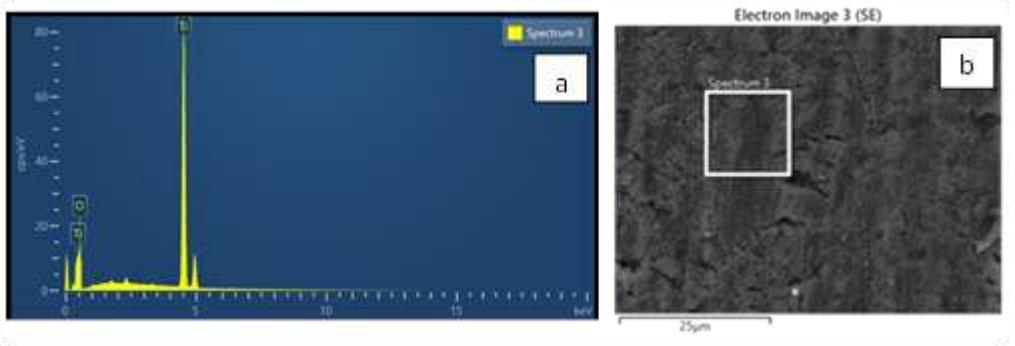

Figure 4.3. (a) EDX spectrum; (b) analysed area of undoped TiO_2nanotbes.

3.4 Antibacterial Analysis

The zones of inhibition (mean ± SD) derived from disk diffusion tests assessing the antibacterial activity of the bare and doped TiO_2 nanotubes are summarized in Table 4 and figure 5. With an inhibitory zone of 29.25 ± 0.35 mm, the silver-doped sample (S) showed the strongest antibacterial activity, significantly outperforming the naked sample (18.60 ± 0.35 mm). The zirconia-graphene (ZG) displayed moderate antibacterial activities with a zone of inhibition of 21.60 ± 4.38 mm, while graphene (G) and zirconia (Z) doped samples showed intermediate activity. These findings demonstrate how silver doping significantly improves antibacterial qualities, most likely as a result of membrane rupture and ion release mechanisms.

Sample Code	**Sample Description**	**Zone of Inhibition (mm) Mean±SD**
ZG	TiO_2 doped with silver	29.25 ± 0.35
S	TiO_2 doped with zirconia-graphene	21.60 ±4.38
G	TiO_2 doped with Graphene	19.95 ± 1.06
Z	TiO_2 doped with Zirconia	19 ± 0.84
B	Bare sample	18.6±0.35

The bare TiO_2 nanotube arrays showed the least inhibition in comparison, highlighting the significance of doping for antibacterial enhancement. The bare TiO_2 nanotube arrays showed the least inhibition in comparison, highlighting the significance of doping for antibacterial enhancement. Zirconia-graphene composite dopants' synergistic actions further imply integrated mechanisms of bacterial inactivation. These findings are further supported by microscopic antibacterial images(Figure5), which demonstrate a distinct rupture of the bacterial membrane and decreased cell viability, particularly in the sample doped with silver. The outcomes are consistent with earlier research highlighting the enhanced antibacterial efficacy of silver-doped nanostructures produced through in situ anodization [36-40]. All things considered, these findings show that doping techniques greatly enhance the antibacterial activity of TiO_2 nanotube surfaces, which is important for biomedical implant applications.

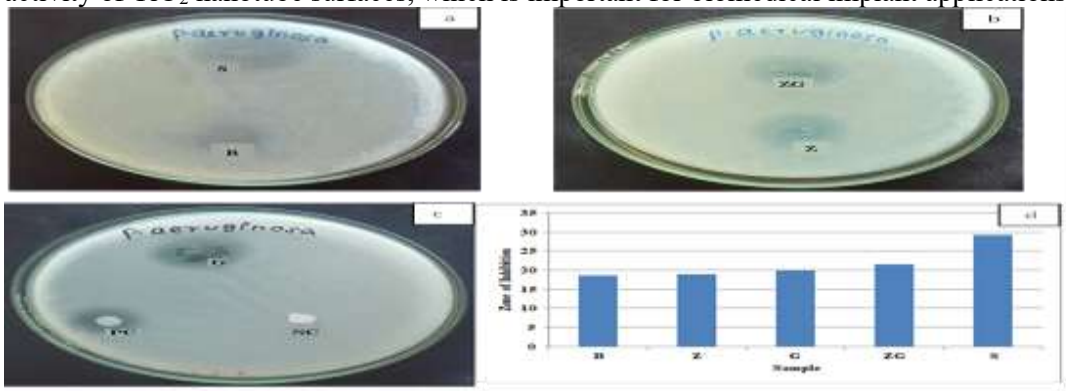

Figure 5.Antibacterial activity of different doped and undoped samples against.Pseudomonas aeruginosa.(a) Bare sample (B) and silver-doped sample (S).(b)Zirconia-doped sample (Z) and zirconia-graphene doped sample(ZG) (c) Graphene-doped sample(G) with positive control (PC) and negative control (NC) (d) Bar graph showing the comparative zone of inhibition (mm) for all samples- B: bare,Z: zirconia-doped, G:graphene-doped,ZG:Zirconia-graphene-doped,and S: silver-doped sample.

3.5 Antbiofilm Analysis

The antibiofil efficacy of silver (S) and zirconia-graphene (ZG) doped TiO2 samples against Pseudomonas aeruginosa (MTCC 424) was assessed using a microtiter plate (MTP) assay.Gentamicin served as the positive control in the experiments. The biofilm biomass was quanified by measuring the optical density at 600 nm after staining with crystal violet dye. A microtiter plate (MTP) test was used to evaluate the antibiofilm activity of the silver (S) and zirconia-graphene (ZG) doped TiO_2 samples against Pseudomonas aeruginosa (MTCC 424), with the antibiotic serving as a positive control. Optical density (OD) measurements at 600 nm and crystal violet staining were used to quantify the biomass of the biofilm [41]. The untreated control had a mean OD of 1.255, indicating strong biofilm development. Biofilm formation was successfully inhibited by gentamicin treatment, as evidenced by a mean OD of 0.044 and a 96.44% inhibition rate. Of the test samples, the zirconia-graphene sample (ZG) had lower antibiofilm activity (mean inhibition : 54.62%) than the silver-doped sample (S), which had higher antibiofilm activity (mean inhibition : 67.18%) (figure 6), because silver ions are known to disturb bacterial membranes and enzymatic processes that are necessary for the stability of biofilms, silver doping has been shown to be remarkably effective. The results of the dose-response study showed concentration-dependent inhibition, with an IC_{50} value of 353.6 μg/mL and a strong fit (R^2=0.9618). Once the concentration threshold is exceeded, a coordinated biofilm disruption response is reflected in the steep Hill slope (41.1). The broad confidence intervals for IC_{50}, however, point to variability that might result from experimental settings or biological heterogeneity [42]. The promise of nanomaterial-based approaches for antibiofilm interventions is highlighted by these findings. Future research might concentrate on improving composite formulations and doping concentrations to increase efficacy and lower variability. The findings encourage further research into these nanomaterials as supplemental or substitute medicines against infections linked to biofilm, given their potential clinical uses.

Table 5. OD values at 600 nm for biofilm quantification by microtiter plate assay showing triplicate readings and mean values for control, antibiotic, ZG and S samples

S.No	Tested Sample	OD Value at 600 nm (in triplicates)	Mean OD
1	Control	1.265,1.229,1.272	1.255
2	Antibiotic	0.054,0.039,0.041	0.044

3	ZG	0.578,0.549,0.582	0.570
4	S	0.389,0.428,0.419	0.412

Table 6.Percentage of biofilm inhibition by tested treatments against P.aeruginosa

S.No	Testes sample	% inhibition (triplicates)	Mean inhibition	IC_{50} (µg/mL)
1	Antibiotic	95.698, 96.893, 96.734	96.44	—
2	ZG	53.96, 56.27, 53.64	54.62	353.6
3	S	69.01, 65.91, 66.62	67.18	353.6

4. Conclusion

In order to look into the antibacterial functions of silver,zirconia,and graphene dopants,this study effectively produced and evaluated undoped and multidoped TiO_2 nanotube arrays via the insitu anodization method. Pseudomonas aeruginosa membrane rupture and the widest zone of inhibition indicated that silver-doped TiO2 has the strongest antibacterial activity. Zirconia-graphene co-doped TiO_2,on the other hand, is a new and promising method despite exhibiting only moderate antibacterial and antibiofilm properties. The combined benefits of graphene's antibiofilm qualities and zirconia's increased mechanical stability open the gate to enhanced long-term implant surface durability and infection resistance.

Anatase phase retention and successful dopant incorporation were confirmed by structural investigations, which increased biointerface interactions and produced a desirable nanotube shape. The $IC_{50}$and concentration-dependent biofilm inhibition underline these multipurpose therapeutic uses. In relation to the current challenges with antibiotic resistance, these results emphasize the significance of employing multifunctional doped TiO2 nanotubes to eradicate implant-associated infections.

In order to enhance therapeutic translation, future research should concentrate on maximizing dopant concentrations, refining composite formulations, and performing comprehensive cytocompatibility and in vivo assessments.

References

1. Mendelson, M. (2015). The World Health Organization Global Action Plan for antimicrobial resistance. South African Medical Journal, 105(5), 325. https://doi.org/10.7196/samj.9644

2. Blair JMA, Webber MA, Baylay AJ, Ogbolu DO, Piddock LJV. Molecular mechanisms of antibiotic resistance. Nature Reviews Microbiology.2015;13: 42-51. https://doi.org/10.1038/nrmicro3380

3. Cassini, A., Högberg, L. D., Plachouras, D., Quattrocchi, A., Hoxha, A., Simonsen, G. S., Colomb-Cotinat, M., Kretzschmar, M. E., Devleesschauwer, B., Cecchini, M., Ouakrim, D. A., Oliveira, T. C., Struelens, M. J., Suetens, C., & Monnet, D. L. (2019). Attributable deaths and disability-adjusted life-years caused by infections with antibiotic-resistant bacteria in the EU and the European Economic Area in 2015: A population-level modelling analysis. The Lancet Infectious Diseases, 19(1), 56–66. https://doi.org/10.1016/S1473-3099(18)30605-4

4. Tacconelli E, Carrara E, Savoldi A, et al. Discovery, research and development of new antibiotics: the WHO priority list of antibiotic-resistant bacteria and tuberculosis, Lancet Infect Dis.2018;18(3):318-327. https://doi.org/10.1016/S1473-3099(17)30753-3
5. Theuretzbacher U, Outterson K, Engel A.,Karlen A. The global preclinical antibacterial pipeline. Nat Rev Microbiol.2020:18:275-285. https://doi.org/10.1038/s41579-019-0288-0
6. Collignon P, Beggs JJ, Walsh TR, Gandra S,Laxminarayan R. Anthropological and socioeconomic factors contributing to global antimicrobial resistance: a Univariate and multivariable analysis.Lancet Planet Health.2018;2(9):e398-e405. https://doi.org/10.1016/S2542-5196(18)30186-4
7. Flemming HC, Wingender J, Szewzyk U, et al. Biofilms: an emergent form of bacterial life. Nat Rev Microbiol. 2016;14:563-575. https://doi.org/10.1038/nrmicro.2016.94
8. Hetrick EM, Schoenfisch MH. Reducing implant-related infections: active release strategies.Chem Soc Rev. 2006;35(9): 780-789. https://doi.org/10.1039/B515219B
9. Roy P, Berger S, Schmuki P. TiO2 nanotubes: synthesis and applications. Angew Chem Int Ed Engl.2011;50(13):2904-2939. https://doi.org/10.1002/anie.201001374
10. Cheng, Y., Yang, H., Yang, Y., Zhang, J., Cao, W., Jiang, D., ... & Liu, X. (2018). Progress in TiO2 nanotube coatings for biomedical applications: A review. Journal of Materials Chemistry B, 6(13), 1862-1886.https://doi.org/10.1039/C8TB00149A
11.Schmuki P,et al.Self-organized anodic TiO2 nanotubes: synthesis and applications.Electrochim Acta. 2005;50(27):5623-5630.https://doi.org/10.1016/j.electacta.2005.04.002
12. Alivov Y, Fan Z. Anodization of Ti in NH4Cl-containing electrolytes: role of chloride ions in nanotube morphology. Electrochim Acta.2009;54(23):5500-5506. https://doi.org/10.1016/j.electacta.2009.04.057
13.Rai M,Yadav A, Grade A. Silver nanoparticles as a new generation of antimicrobials.Biotechnol Adv.2009;27(1):76-83. https://doi.org/10.1016/j.biotechadv.2008.09.002
14. Aydın, S., et al. (2018). Antibacterial activity of silver-doped TiO2 nanotubes. Applied Surface Science, 455, 469-480. https://doi.org/10.1016/j.apsusc.2018.06.007
15. Han, H., et al. (2021). Ag-doped TiO2 nanofilms with 99.7% antibacterial efficiency for vascular implants. Advanced Materials Interfaces, 8(19), 2100892. https://doi.org/10.1002/admi.202100892
16. Yao, Y., Lin, P., Ye, D., Miao, H., Cao, L., Zhang, P., Xu, J., & Dai, L. (2025). Enhanced long-term antibacterial and osteogenic properties of silver-loaded titanium dioxide nanotube arrays for implant applications. International Journal of Nanomedicine, 20, 3749–3764. https://doi.org/10.2147/IJN.S493754
17. Khan, S., et al. (2020). Zirconia-based nanomaterials with antimicrobial properties. ACS Omega, 5(5), 2546-2554. https://doi.org/10.1021/acsomega.9b03840
18. Staneva, A. D., Dimitrov, D. K., Gospodinova, D. N., & Vladkova, T. G. (2021). Antibiofouling activity of graphene materials and graphene-based antimicrobial coatings. Microorganisms, 9(9), Article 1839. https://doi.org/10.3390/microorganisms9091839
19. Christensen, G. D., Simpson, W. A., Younger, J. J., Baddour, L. M., Barrett, F. F., Melton, D. M., & Beachey, E. H. (1985). Adherence of coagulase-negative staphylococci to plastic tissue culture plates: A quantitative model for the adherence of staphylococci to

medical devices. Journal of Clinical Microbiology, 22(6), 996-1006. https://doi.org/10.1128/JCM.22.6.996-1006
20. Yin, S., Zhang, Q., Sato, T., & Sekino, T. (2001). Low-temperature synthesis of nanocrystalline anatase TiO_2 by hydrothermal treatment of $TiCl_4$ and NH_3. Materials Chemistry and Physics, 72(1), 25-29. https://doi.org/10.1016/S0254-0584(01)00258-4
21.Shao, D., Zhang, J., Chen, C.,Li,J.,& Xie, J.(2009). The effect of silver loading on TiO2 nanotube arrays for photocatalytic hydrogen production. Applied Surface Science, 255(10),5015-5020.https://doi.org/10.1016/j.apsusc.2008.12.031
22. Shin, H.J.,Kim, K.K., Benayad,A., Yoon, S.M.Park, H.K., Jung,I.S.,&Lee,Y.H.(2009).Efficient reduction of graphene oxide by sodium borohydride and its effect on electrical conductance.Applied Physics Letters,95(15),153103. https://doi.org/10.1063/1.3247964
23 Katal, R., Ghasemi, M., Esfandiari, N., & Azizi, M. (2020). Structural and photocatalytic performance of Zr-doped TiO_2 nanotubes. Journal of Materials Science: Materials in Electronics, 31(12), 10032-10045. https://doi.org/10.1007/s10854-020-03615-y
24. Palmisano,L., Augugliaro, V.,Pagliaro,M, & Palmisano,G.(2004). Effect of zirconia addition on the photocatalytic activity of nanocrystalline TiO2.Applied catalysis B: Environmental,48(1) 49-63. https://doi.org/10.1016/j.apcatb.2004.06.010
25.Paulose,M., Varghese,O.K., & Grimes, C.A.(2007).TiO2 nanotube arrays of 1000μm length by anodization of titanium foil.The Journal of Physical Chemistry C, 111(44),14992-15007. https://doi.org/10.1021/jp075258r
26. Patil, R. R., Kamat, A. D., & Bhanvase, B. A. (2021). Field emission characteristics of double-walled TiO2 nanotubes. ES Materials & Manufacturing, 13, 76-81. https://doi.org/10.3934/matersx.2015.2.460
27. Ramakrishnan, V., Sankaranarayanan, V., & Narayan, R. (2020). Effects of graphene oxide doping on TiO_2 nanotubes growth and photocatalytic performance. *Chemical Engineering Journal*, 382, Article 123054. https://doi.org/10.1016/j.cej.2019.123054
28. Moridon, S., Gao, F., & Li, J. (2023). Silver-doped TiO2 nanotubes for enhanced antimicrobial effects. Nanomaterials, 13(5), 959. https://doi.org/10.3390/nano13050959
29. Lai,H.,Zhang,W.,& Yin, F.(2014).Zirconia doping enhanced mechanical properties of TiO2 nanotubes.Journal of Photochemistry and Photobiology A:Chemistry,281,17-22. https://doi.org/10.1016/j.jphotochem.2014.01.012
30. Zalnezhad, E., Ahmad, A.,& Ong, M.T.(2016). Corrosion and antibacterial properties of doped TiO_2 nanotubes. Corrosion Science, 105,74-84. . https://doi.org/10.1016/j.corsci.2015.12.009
31. Wang, Y.,Lee.,& Mazare, A..(2012). Silver-doped TiO2 nanotube arrays for enhanced antibacterial activity. Journal of Biomedical Materials Research Part A,100A(2),528-534. https://doi.org/10.1002/jbm.a.33281
32. Sulka, G.D., Kapusta-Kolodziej,J., Brzozka, A.,& Jaskula,M.(2011).Electrochemical fabrication of zirconium-doped TiO2 nanotubes and their application in dye-sensitized solar cells. Electrochimica Acta, 56(13),4972-4979.https://doi.org/10.1016/j.electacta.2011.02.085
33. Pan, X., Yang,M.Q.,Fu, X., Zhang, N.,&Xu,Y.J.(2012). Synergistic effect of graphene and Zr doping on phoocatalytic performance of TiO2. Applied Catalysis B: Environmental,111-112, 288-296.https://doi.org/10.1016/j.apcatb.2011.10.028

34. Li, J., et al. (2018). Enhanced antibacterial activity of silver-doped titanium dioxide–chitosan composites under visible light. Materials, 11(8), 1403. https://doi.org/10.3390/ma11081403
35. Serov, D. A., Gritsaeva, A. V., Yanbaev, F. M., Simakin, A. V., & Gudkov, S. V. (2024). Review of antimicrobial properties of titanium dioxide nanoparticles: Effect of size, shape, and doping. International Journal of Molecular Sciences, 25(19), Article 10519. https://doi.org/10.3390/ijms251910519
36. Ghdeeb, N. J., & Abdalameer, N. K. (2024). Synthesis, characterization, and antimicrobial activity of CuO nanoparticles and CuO/Ag nanocomposites. Applied Nanoscience, 14(2), 401-409. https://doi.org/10.1007/s13204-023-02984-2
37. Sondezi, N., Ngcobo, S., Ngubane, T., et al. (2024). Sol-gel derived TiO2 and TiO2/Cu nanoparticles: Synthesis, characterization, and antibacterial efficacy. ACS Omega, 9(14), 16234-16245. https://doi.org/10.1021/acsomega.3c09308
38. Khan MU, Rehman W, Bibi S, Alanazi MM, Alanazi AS, Rasheed L, Khan S, Gillani SUT, Tauqeer A, Synthesis, Characterization, and antimicrobial and nematicidal activities of chitosan- based silver-doped titanium dioxide.ACS Omega 2023;8(21): 18745-18755.https://doi.org/10.1021/acsomega.3c00068
39.da Costa Lima, J.L., Alves LR, da Paz JNP, RabeloMA, Maciel MAV, de Morais MMC, (2017). Analysis of biofilm production by clinical isolates of Pseudomonas aeruginosa from patients with ventilator-associated pneumonia,Rev Bras TerIntensiva, 29(3), 310-316. https://doi.org/10.5935/0103-507X.20170039
40. Shrestha, S., Shrestha, L. B., & Kayestha, S. (2021). Detection of biofilm formation among Pseudomonas aeruginosa isolated from burn patients. Burns Open, 2(3), 128-133. https://doi.org/10.1016/j.burnso.2021.04.001